Mon. Not. R. Astron. Soc. **365,** 1333–1347 (2006) doi:10.1111/j.1365-2966.2005.09824.x

The maximum stellar mass, star-cluster formation and composite stellar populations

Carsten Weidner[1,2]★ and Pavel Kroupa[1,2]★

[1]*Argelander Institut für Astronomie (Sternwarte), Universität Bonn, D-53121 Bonn, Germany*
[2]*The Rhine-Stellar-Dynamical Network*

Accepted 2005 November 1. Received 2005 October 29; in original form 2005 July 15

ABSTRACT

We demonstrate that the mass of the most massive star in a cluster correlates non-trivially with the cluster mass. A simple algorithm, according to which a cluster is filled up with stars that are chosen randomly from the standard initial mass function (IMF) but sorted with increasing mass, yields an excellent description of the observational data. Algorithms based on random sampling from the IMF without sorted adding are ruled out with a confidence larger than 0.9999. A physical explanation of this would be that a cluster forms by more-massive stars being consecutively added until the resulting feedback energy suffices to revert cloud contraction and stops further star formation. This has important implications for composite populations. For example, 10^4 clusters of mass $10^2\,\mathrm{M}_\odot$ will not produce the same IMF as one cluster with a mass of $10^6\,\mathrm{M}_\odot$. It also supports the notion that the integrated galaxial stellar IMF (IGIMF) should be steeper than the stellar IMF and that it should vary with the star formation rate of a galaxy.

Key words: stars: formation – stars: luminosity function, mass function – Galaxy: stellar content – galaxies: evolution – galaxies: star clusters – galaxies: stellar content.

1 INTRODUCTION

The insight that clustered star formation may be the dominant mode for star formation has grown over the last years. The form of the true distribution of stellar masses within these clusters, of the stellar initial mass function (IMF), has been a subject of debate for a long time. The evolution of the stars, unresolved binaries, and the dynamical evolution of the clusters complicate the observational efforts to extract the IMF. Unfortunately, the most promising objects, very young stellar clusters (age < 3 Myr), are often still embedded in their natal cloud – again aggravating observations.

Nevertheless, the distribution of stars in young clusters seems to be fairly well described by a multiple power-law function with a slope or index (α) of 2.35 (the so-called 'Salpeter' value) for stars with a mass larger than $0.5\,\mathrm{M}_\odot$ (Kroupa 2001). The IMF,

$$\xi(m) \propto m^{-\alpha_i}, \tag{1}$$

where $\xi(m)\,\mathrm{d}m$ is the number of stars in the mass interval $[m, m + \mathrm{d}m]$. Several observations find the Salpeter value ($\alpha_3 = 2.35$) for a large variety of conditions (Massey & Hunter 1998; Sirianni et al. 2000, 2002; Parker et al. 2001; Massey 2002, 2003; Wyse et al. 2002; Bell et al. 2003; Piskunov et al. 2004). It is therefore useful to describe the *stellar IMF* with an invariant, multiple power-law form (Kroupa, Tout & Gilmore 1993; Kroupa 2001; Reid, Gizis & Hawley 2002),

$$\begin{aligned}
\alpha_0 &= +0.30 \quad 0.01 \leqslant m/\mathrm{M}_\odot < 0.08,\\
\alpha_1 &= +1.30 \quad 0.08 \leqslant m/\mathrm{M}_\odot < 0.50,\\
\alpha_2 &= +2.35 \quad 0.50 \leqslant m/\mathrm{M}_\odot < 1.00,\\
\alpha_3 &= +2.35 \quad 1.00 \leqslant m/\mathrm{M}_\odot.
\end{aligned} \tag{2}$$

We refer to this form as the standard or canonical stellar IMF because this form fits the luminosity function of Galactic field and cluster stars below $1\,\mathrm{M}_\odot$ and also represents young populations above $1\,\mathrm{M}_\odot$ (Kroupa et al. 1993; Kroupa 2001, 2002). As pointed out by Scalo (1998, 2005) though, significant uncertainties remain in the determination of the IMF to the point that the case can also be made that a single form of the IMF may not exist. In view of this, the ansatz made here and elsewhere is to propose the hypothesis of an invariant standard or canonical IMF (equation 2) and to test if the variation of the observed IMF can be understood to be the result of astrophysical effects (obscuration, stellar evolution, and stellar multiplicity), dynamical effects (mass segregation, stellar evaporation and ejections), stochastic effects (finite N-sampling from the IMF) and the construction of composite populations (addition of many different clusters).

Similarly, the embedded cluster mass function (ECMF) has been found to be well described by at least one power law,

$$\xi_{\mathrm{ecl}}(M_{\mathrm{ecl}}) \propto M_{\mathrm{ecl}}^{-\beta}, \tag{3}$$

★E-mail: cweidner@astro.uni-bonn.de (CW); pavel@astro.uni-bonn.de (PK)

where $\mathrm{d}N_{\rm ecl} = \xi_{\rm ecl}\,(M_{\rm ecl})\,\mathrm{d}M_{\rm ecl}$ is the number of embedded clusters in the mass interval $[M_{\rm ecl}, M_{\rm ecl} + \mathrm{d}M_{\rm ecl}]$ and $M_{\rm ecl}$ is the cluster mass in stars. The observational evidence points to a possibly universal form of the ECMF: Lada & Lada (2003) find a slope $\beta = 2$ in the solar neighbourhood for clusters with masses between 50 and 1000 $\mathrm{M}_\odot$, while Hunter et al. (2003) find $2 \lesssim \beta \lesssim 2.4$ for $10^3 \lesssim M_{\rm ecl}/\mathrm{M}_\odot \lesssim 10^4$ in the Small Magellanic Cloud (SMC) and Large Magellanic Cloud (LMC), and Zhang & Fall (1999) find 1.95 ± 0.03 for $10^4 \lesssim M_{\rm ecl}/\mathrm{M}_\odot \lesssim 10^6$ in the Antennae galaxies. Weidner, Kroupa & Larsen (2004) discovered that $\beta = 2.35$ best reproduces the observed correlation between the brightest young cluster and the galaxy-wide star formation rate (SFR) for a large sample of late-type galaxies.

As already mentioned by Vanbeveren (1982) and discussed in more detail by Kroupa & Weidner (2003), the composite or integrated galaxial stellar IMF (IGIMF) is obtained by summing up the stellar IMFs contributed by all the star clusters that formed over the age of a galaxy,

$$\xi_{\rm IGIMF}(m;t) = \int_{M_{\rm ecl,min}}^{M_{\rm ecl,max}(SFR(t))} \xi(m \leqslant m_{\rm max}(M_{\rm ecl}))\,\xi_{\rm ecl}(M_{\rm ecl})\,\mathrm{d}M_{\rm ecl}, \quad (4)$$

where $\xi_{\rm ecl}(M_{\rm ecl})$ is the ECMF and $\xi[(m \leqslant m_{\rm max}(M_{\rm ecl})]$ is the stellar IMF in a particular cluster within which the maximal mass of a star is $m_{\rm max}$. $M_{\rm ecl,min}$ ($=5\,\mathrm{M}_\odot$, Taurus–Auriga type 'clusters') is the minimal cluster mass, while the maximal cluster mass, $M_{\rm ecl,max}$, depends on the galaxy-wide SFR (Weidner et al. 2004).

A critical function entering this description is thus $m_{\rm max}\,(M_{\rm ecl})$. Assuming the stellar IMF to be a continuous distribution function, this mass of the most massive star in an embedded cluster with the total mass $M_{\rm ecl}$ in stars is given by

$$1 = \int_{m_{\rm max}}^{m_{\rm max*}} \xi(m)\,\mathrm{d}m, \quad (5)$$

with

$$M_{\rm ecl} = \int_{m_{\rm low}}^{m_{\rm max}} m\,\xi(m)\,\mathrm{d}m, \quad (6)$$

since there exists exactly one most massive star in each cluster, and neglecting statistical variations. Here $m_{\rm low} = 0.01\,\mathrm{M}_\odot$ is the minimal fragmentation mass and $m_{\rm max*} \approx 150\,\mathrm{M}_\odot$ is the measured maximal stellar mass limit (Weidner & Kroupa 2004; Figer 2005; Oey & Clarke 2005). On combining equations (5) and (6) the function

$$m_{\rm max} = {}^{l}m^{\rm ana}_{\rm max}(M_{\rm ecl}) \quad (7)$$

is quantified by Weidner & Kroupa (2004) and discussed in Section 2. This is the analytical (ana) maximum stellar mass–cluster mass relation which incorporates the fundamental stellar upper mass limit (noted by the leading superscript 'l') of $m_{\rm max*} = 150\,\mathrm{M}_\odot$. Later on other maximum stellar mass–cluster mass relations are indicated by different superscripts: 'ran', 'con' and 'sort' for the different Monte Carlo sampling methods (see Section 2.2) and also 'u' for the case without a fundamental stellar upper mass limit.

Weidner & Kroupa (2004) infer that a fundamental upper stellar mass limit, $m_{\rm max*} \approx 150\,\mathrm{M}_\odot$, appears to exist above which stars do not occur, unless $\alpha_3 \gtrsim 2.8$, in which case no conclusions can be drawn based on the expected number of massive stars. As reviewed by Kroupa & Weidner (2005), the existence of such a stellar upper mass limit has been further substantiated by Figer (2005) and Oey & Clarke (2005) for a range of star clusters and OB associations.

We thus have, for each $M_{\rm ecl}$, the maximal stellar mass, $m_{\rm max}(M_{\rm ecl}) \leqslant m_{\rm max*}$, and with this information equation (4) can be evaluated to compute the IGIMF. Kroupa & Weidner (2003) find the IGIMF, when evaluated to the highest-cluster masses, to be significantly steeper than the stellar IMF, and Weidner & Kroupa (2005) extend the analysis to a time-varying ECMF by noting that $M_{\rm ecl,max}$ increases with the SFR of a galaxy. They show the IGIMF to be not only steeper than the stellar IMF, but also to depend on galaxy type. The implications of these findings are rather significant for the supernova rate (Weidner & Kroupa 2005) and for the chemical evolution of galaxies (Köppen, Weidner & Kroupa 2006).

But these results do not remain without a challenge. Elmegreen (2005) argues that there is no evidence of a relation $m_{\rm max} = m_{\rm max}(M_{\rm ecl}) \leqslant m_{\rm max*}$. This relation implies that many small, low-mass, star-forming events will not have the same combined IMF as one major star-forming event of the same mass. Thus, according to Kroupa & Weidner (2005), 10^5 clusters each with a mass of $20\,\mathrm{M}_\odot$ would provide a combined IMF that differs from that of one cluster with a mass of $2 \times 10^6\,\mathrm{M}_\odot$ by being under-represented in stars with a mass above approximately $m_{\rm max} = 1\,\mathrm{M}_\odot$. The contrary, often voiced view is that stellar masses sample the IMF purely statistically such that 10^5 clusters containing 50 stars (on average $20\,\mathrm{M}_\odot$) will give the same combined IMF as one cluster containing 5×10^6 stars (Elmegreen 1999, 2005).

With this contribution we demonstrate conclusively that the purely statistical notion is false, and that the stellar IMF is sampled to a maximum stellar mass that correlates with the cluster mass. Therewith we affirm the results obtained by Kroupa & Weidner (2003) and Weidner & Kroupa (2005), and we also attain useful insights into the process of star-cluster formation.

In Section 2, our Monte Carlo procedure is described and the maximal star mass–cluster mass relation is derived, while in Section 3 the Monte Carlo experiment is applied to the IGIMF and the results are presented. A discussion with conclusions is available in Section 4.

2 THE MAXIMAL STAR MASS IN A CLUSTER

2.1 Previous studies

Over the past 20 yr several studies investigated a possible connection of the maximum stellar mass in a cluster and the mass of the cluster because such a relation, if it were to exist, would allow important insights into the star formation process.

Larson (1982) compared the properties of molecular clouds with the spatial distribution of the associated stellar population. He found that more-massive and dense clouds favour the formation of massive stars and fitted the following formula to the observations,

$$m_{\rm max} = 0.33 M_{\rm cloud}^{0.43}. \quad (8)$$

He re-evaluated (Larson 2003) this equation with more recent data and applied it directly to the cluster mass instead of the cloud mass,

$$m_{\rm max} = 1.2 M_{\rm ecl}^{0.45}. \quad (9)$$

This correlation is plotted as a dotted line in Figs 1 and 7.

Elmegreen (1983) proposed a model for the origin of bound galactic clusters where the luminosity of the stars from a Miller & Scalo (1979) IMF overcomes the binding energy of a molecular cloud core. The star formation efficiency then discriminates between bound clusters and OB associations. He derived an analytical estimate for a relation between the maximal star mass and the cluster

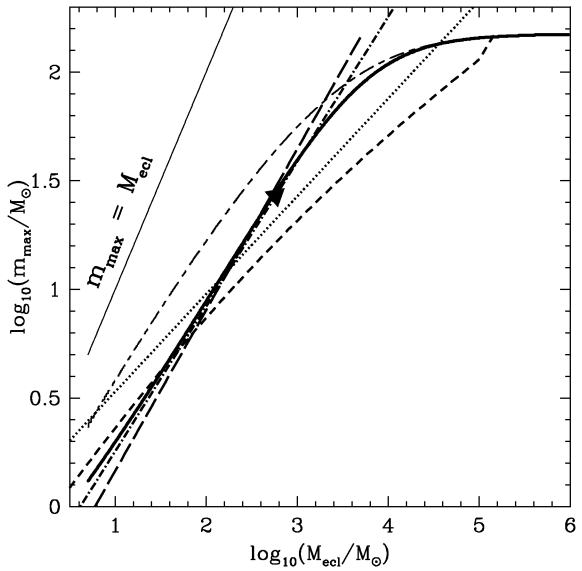

Figure 1. The maximal star mass, $m_{\rm max}$, in dependence of the cluster mass, $M_{\rm ecl}$, both in logarithmic units. The Larson (2003) relation (equation 9) is shown as a dotted line, while the Elmegreen (1983) relation (equation 10) is the short-dashed line. The Elmegreen (2000) relation (equation 12) is the long-dashed line. The result (equation 13) from numerical SPH star formation simulations (Bonnell et al. 2004) is plotted as a short-dashed–dotted line and as a *triangle* for a specific model from Bonnell et al. (2003), while the long-dashed–short-dashed line marks the expectation values (equation 14) from Oey & Clarke (2005) and the thick solid line shows the semi-analytical model (equation 7) of Weidner & Kroupa (2004) for the standard IMF (equation 2). The thin solid line shows the identity relation, were a 'cluster' consists of only one star.

mass from statistical considerations regarding the appearance of stars with various masses from the Miller–Scalo IMF,

$$M_{\rm ecl} = \frac{{\rm e}^{A_2}\, F[A_1(\log m_{\rm max} - A_3)]}{1 - F[A_1(\log m_{\rm max} - C_2)]}, \tag{10}$$

with

$$F(x) = (2\pi)^{-1/2} \int_{-\infty}^{x} {\rm e}^{(-t^2/2)}\, {\rm d}t, \tag{11}$$

and $A_1 = (2C_1)^{1/2}$, $A_2 = \ln 10\,(C_2 + \ln 10/4C_1) = -1.064$, $A_3 = C_2 + \ln 10/2C_1 = 0.065$, $C_1 = 1.09$ and $C_2 = -0.99$. In Figs 1 and 7 this relation is shown as a short-dashed line.

On the other hand, using a single power-law IMF with a Salpeter (1955) slope, Elmegreen (2000) solved equations (5) and (6), assuming $m_{\rm max*} = \infty$, with the result,

$$M_{\rm ecl} = 3 \times 10^3 \left(\frac{m_{\rm max}}{100\,{\rm M}_\odot}\right)^{1.35} {\rm M}_\odot, \tag{12}$$

which is shown as a long-dashed line in Figs 1 and 7.

Bonnell, Bate & Vine (2003) and Bonnell, Vine & Bate (2004) numerically studied star formation in clusters using their smoothed particle hydrodynamics (SPH) code. Here a turbulent molecular cloud fragments hierarchically into smaller subunits. When the density of a clump gets higher than a critical value, it is replaced by a so-called 'sink' particle which only lets matter in but not out. These sink particles form the final stellar cluster by interactions and mergers and are called stars at the end of the simulation. This hierarchical cluster formation scenario leads to the relation,

$$m_{\rm max} \propto M_{\rm ecl}^{2/3}, \tag{13}$$

and is shown as a short-dashed–dotted line in Figs 1 and 7. There equation (13) is normalized to $m_{\rm max} = 27$ for a cluster of $M_{\rm ecl} = 580\,{\rm M}_\odot$ (Bonnell et al. 2003, 2004). It should be noted here that these simulations do not include magnetic fields, stellar feedback and stellar mergers, all of which are believed to be of great importance for star formation.

Weidner & Kroupa (2004) started with similar assumptions as Elmegreen (2000) but included a physical upper limit for the stellar mass, $m_{\rm max*} = 150\,{\rm M}_\odot$, while solving equations (5) and (6). Due to $m_{\rm max*}$ and using the standard multiple power-law IMF (equation 2), the result cannot be written out analytically but the equations have to be solved numerically. The result is plotted as a thick solid line in Figs 1 and 7.

In a broader statistical analysis, Oey & Clarke (2005) calculated the probabilities that the observed upper mass limits in several clusters and OB associations in the Milky Way (MW), LMC and SMC come from a sample with a fundamental upper mass limit, $m_{\rm max*}$, or not. They conclude that an upper mass limit between 120 and 200 $\,{\rm M}_\odot$ is the most likely explanation for the observed maximum masses. In order to do so, they calculated the expectation value for the maximum mass if a number N of stars is randomly sampled from an IMF. This yields the equation,

$$\langle m_{\rm max}\rangle = m_{\rm max*} - \int_0^{m_{\rm max*}} \left[\int_0^{M_{\rm ecl}} \xi(m)\,{\rm d}m\right]^N {\rm d}M_{\rm ecl}. \tag{14}$$

Integrating this numerically yields the long-dash–short-dashed line in Figs 1 and 7 assuming $m_{\rm max*} = 150\,{\rm M}_\odot$.

2.2 Monte Carlo experiments

All the above mentioned investigations suggest that the cluster mass indeed appears to have a limiting influence on the stellar masses within it. However, it would be undisputed that a stochastic sampling effect from the IMF must be present when stars form. To investigate the possible existence of a maximal stellar mass in clusters statistically and to confirm or rule out if such a relation is purely the result of the random selection from an IMF, following three Monte Carlo experiments are conducted.

(i) Pure random sampling (random sampling);
(ii) mass-constrained random sampling (constrained sampling); and
(iii) mass-constrained random sampling with sorted adding (sorted sampling).

For each, two possibilities are probed: stars are sampled from the IMF without a maximal mass ($m_{\rm max*} = \infty$[1]), or their masses are limited by $m_{\rm max*} = 150\,{\rm M}_\odot$.

2.2.1 *Random sampling*

For the random-sampling experiment, 2.5×10^7 clusters are randomly taken from a cluster distribution with a power-law index $\beta_N = 2.35$. The clusters contain between 12 and 2.7×10^7 stars. The relevant distribution function is the embedded-cluster star-number function (ECSNF),

$${\rm d}N_{\rm ecl} \propto N_{\rm stars}^{\beta_N}, \tag{15}$$

[1] For practical reasons of numerical computation $m_{\rm max*}$ is adopted to be $m_{\rm max*} = 10^6\,{\rm M}_\odot$ in the unlimited case.

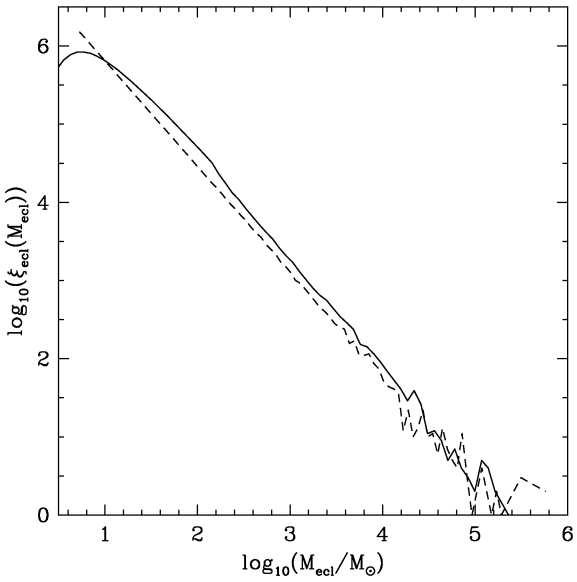

Figure 2. The embedded cluster mass function (ECMF) derived from randomly picking 10^7 clusters using equation (3) (dashed line) and as described in Section 2.2.1 (solid line). The slopes are virtually the same ($\beta_N = \beta$). Only for very small cluster masses does the solid line deviate due to the underlying standard IMF because small-N clusters can nevertheless have masses $> 10\,\mathrm{M}_\odot$ if their constituent stars happen to be massive. This accounts for the turn-down below $10\,\mathrm{M}_\odot$ and the surplus in the range 10–150 $\mathrm{M}_\odot$.

which is the number of clusters containing $N \in [N', N' + \mathrm{d}N']$ stars. Each cluster is then filled with N stars randomly from the standard IMF (equation 2) without a mass limit, or by imposing the physical stellar mass limit, $m \leqslant 150\,\mathrm{M}_\odot$. The stellar masses are then summed up to get the cluster mass, $M_{\rm ecl}$. Note that such a cluster distribution gives an embedded-cluster mass function (ECMF) that is virtually identical to equation (3) (Fig. 2). The resulting distribution of maximum stellar masses is plotted in the $m_{\rm max}$–$M_{\rm ecl}$ plane (Fig. 3) as contour lines, to show the overall distribution (for a more detailed discussion, see Section 2.2.4).

As in this method the higher cluster masses are only very scarcely sampled, a second method is used to evaluate the mean of maximal masses in more detail. In order to do so the cluster star numbers $N = 12$ to 2.7×10^7 are divided into 10 logarithmically equally spaced values. Each of these numbers is then filled 10 000 times with stars from the IMF, keeping only the mass of the most massive star for each cluster. The mean maximum mass for every bin then defines,

$$^{l}\overline{m}^{\rm ran}_{\rm max}(M_{\rm ecl}), \tag{16}$$

with a limit of $m_{\rm max*} = 150\,\mathrm{M}_\odot$ and

$$^{u}\overline{m}^{\rm ran}_{\rm max}(M_{\rm ecl}), \tag{17}$$

in the unlimited case.

2.2.2 *Constrained sampling*

In this case 2.5×10^7 clusters are randomly taken from the ECMF (equation 3) between $5\,\mathrm{M}_\odot$ (the minimal, Taurus–Auriga type, star-forming 'cluster' counting ≈15 stars) and $10^6\,\mathrm{M}_\odot$ (an approximate maximum mass for a single stellar population that consists of one metallicity and age, Weidner et al. 2004; Gieles et al. 2005) and again with $\beta = 2.35$. Note that $\beta_N \approx \beta$ because the ECSNF and the ECMF only differ by a nearly constant average stellar mass

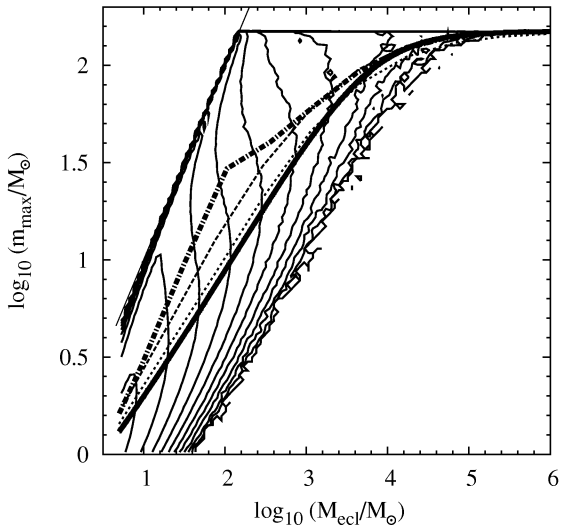

Figure 3. Maximal mass of stars versus cluster mass. The contour lines show how often a certain combination of cluster mass and maximal star mass occurs. The further out they lie (towards the upper right-hand side) the smaller is the number of clusters with this combination. They are spaced logarithmically such that the outermost one represents a single cluster with a certain mass and maximal star ($\log_{10} N_{\rm ecl} = 0$), e.g. $M_{\rm ecl} = 10^5\,\mathrm{M}_\odot$,and $m_{\rm max} \approx 100\,\mathrm{M}_\odot$. The innermost one (near $M_{\rm ecl} = 7\,\mathrm{M}_\odot$, and $m_{\rm max} \approx$ few $\mathrm{M}_\odot$) stands for $\log_{10} N_{\rm ecl} = 4.5$ clusters with this maximal star mass. The lines in between are in steps of 0.5 dex. Here the contour lines are the result of the Monte Carlo simulations with random sampling. The semi-analytic result (equation 7), $^{l}m^{\rm ana}_{\rm max}(M_{\rm ecl})$, is the thick solid line. Mean values are shown as the thick dot–dashed line for random sampling [$^{l}\overline{m}^{\rm ran}_{\rm max}(M_{\rm ecl})$, equation 16], as the thin dashed line for constrained sampling [$^{l}\overline{m}^{\rm con}_{\rm max}(M_{\rm ecl})$, equation 18] and as the thin dotted line for sorted sampling [$^{l}\overline{m}^{\rm sort}_{\rm max}(M_{\rm ecl})$, equation 20]. The identity relation $m_{\rm max} = M_{\rm ecl}$ is plotted as a thin solid line.

(Fig. 2). Then stars are taken randomly from the standard IMF and added until they reach or just surpass the respective cluster mass, $M_{\rm ecl}$. Afterwards the clusters are searched for their maximum stellar mass (plotted as contours in Fig. 4, see Section 2.2.4 for discussion).

Again the sampling of high-cluster masses is very poor. Therefore, the cluster masses from 5 to $10^6\,\mathrm{M}_\odot$ are divided into 10 logarithmically equally spaced values. Then each of these 10 cluster masses is filled 10 000 times with stars from the IMF until their combined mass reaches or just surpasses the cluster mass and only the maximum star mass is recorded. The average $m_{\rm max}$ values for each of the 10 cluster masses define the relation,

$$^{l}\overline{m}^{\rm con}_{\rm max}(M_{\rm ecl}), \tag{18}$$

in the limited case and

$$^{u}\overline{m}^{\rm con}_{\rm max}(M_{\rm ecl}), \tag{19}$$

in the unlimited case.

2.2.3 *Sorted sampling*

For the third method again 2.5×10^7 clusters are randomly taken from the ECMF (equation 3) between 5 and $10^6\,\mathrm{M}_\odot$ and with $\beta = 2.35$. However, this time the number N of stars which are to populate the cluster is estimated from $N = M_{\rm ecl}/m_{\rm av}$, where $m_{\rm av} = 0.36\,\mathrm{M}_\odot$ is the average stellar mass for the standard IMF (equation 2) between 0.01 and $150\,\mathrm{M}_\odot$. These stars are added to

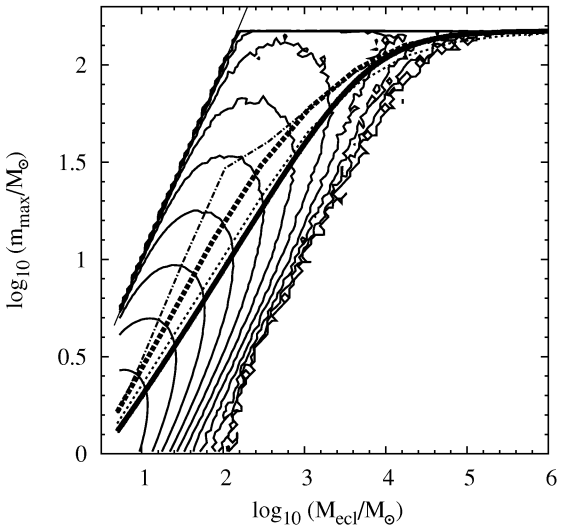

Figure 4. Like Fig. 3 but this time the contour lines are the result of the Monte Carlo simulations with mass-constrained sampling, and ${}^{l}\overline{m}^{\rm con}_{\rm max}(M_{\rm ecl})$ is shown as a thick line, while ${}^{l}m^{\rm ran}_{\rm max}(M_{\rm ecl})$ and ${}^{l}\overline{m}^{\rm sort}_{\rm max}(M_{\rm ecl})$ are shown by thin lines. ${}^{l}m^{\rm ana}_{\rm max}$ is shown by thick solid line.

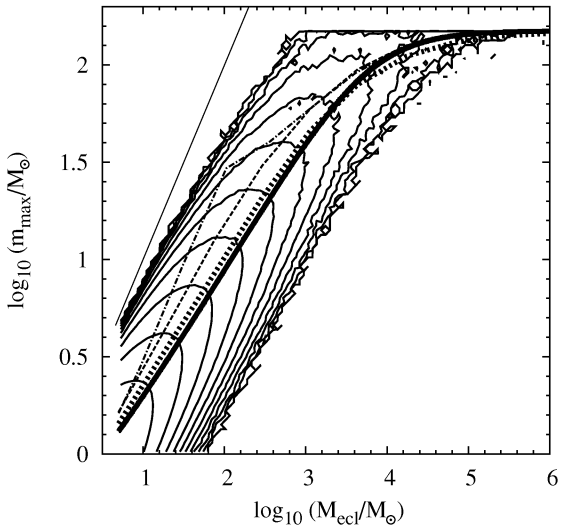

Figure 5. Like Figs 3 and 4 but this time the contour lines are the result of the Monte Carlo simulations with sorted sampling with ${}^{l}\overline{m}^{\rm sort}_{\rm max}(M_{\rm ecl})$ is shown as a thick line.

give $M_{\rm ecl,ran}$,

$$M_{\rm ecl,ran} = \sum_{N} m_i,$$

such that $m_i \leqslant m_{i+1}$. If $M_{\rm ran} < M_{\rm ecl}$ in this first step, an additional number of stars, ΔN, are picked randomly from the IMF, where $\Delta N = (M_{\rm ecl} - M_{\rm ecl,ran})/m_{\rm av}$. Again these stars are added to obtain an improved estimate of the desired cluster mass,

$${}^{*}M_{\rm ecl,ran} = \sum_{N+\Delta N} m_i,$$

again with $m_i \leqslant m_{i+1}$. When ${}^{*}M_{\rm ecl,ran}$ surpasses $M_{\rm ecl}$, it is checked whether the sum is closer to $M_{\rm ecl}$ when the last star (the most massive one) is subtracted or not. If ${}^{*}M_{\rm ecl,ran}$ is closer to $M_{\rm ecl}$ with the last star, this one is the most massive one for the cluster, otherwise it is the second last star.[2] This procedure is followed and repeated until all clusters from the ECMF are 'filled'. The contour plots of the most massive star for each cluster are shown in Fig. 5 and discussed in Section 2.2.4

Again, for a more detailed analysis, 10 cluster masses are generated like in Section 2.2.2 but filled with stars in the sorted way described above. The mean over each of the 10 cluster masses then yields the relation

$${}^{l}\overline{m}^{\rm sort}_{\rm max}(M_{\rm ecl}). \qquad (20)$$

2.2.4 *Comparison of the samplings*

In order to exemplify the differences between the three sampling methods the following gedanken experiment may be considered.

A sample of 10 stars consists of nine stars with $5\,{\rm M}_\odot$ and one with $11\,{\rm M}_\odot$. For the random sampling, this would be a cluster with $M_{\rm ecl,\,ran} = 56\,{\rm M}_\odot$, and with $m_{\rm max,\,ran} = 11\ {\rm M}_\odot$. If, for the sorted sampling, the aimed-at cluster mass is $50\,{\rm M}_\odot$, the actual cluster mass would be $45\,{\rm M}_\odot$ ($= 9 \times 5$), because 45 is closer to 50 than 56, and $m_{\rm max,\,sort}$ would be $5\,{\rm M}_\odot$. In the case of constrained sampling the order would be important. If the aimed-at cluster mass is $50\,{\rm M}_\odot$ and the 11-$\,{\rm M}_\odot$ star is among the first nine stars, $M_{\rm ecl,\,con}$ would be 51 ($= 8 \times 5 + 11$) and $m_{\rm max,\,con} = 11\,{\rm M}_\odot$. But if the 11 - $\,{\rm M}_\odot$ star is the tenth star, $M_{\rm ecl,\,con}$ would be $45\,{\rm M}_\odot$, and $m_{\rm max,\,con} = 5\,{\rm M}_\odot$ as in the sorted-sampling case because, 45, rather than 56, is closer to $50\,{\rm M}_\odot$.

Figs 3, 4 and 5 plot the contour lines of the most massive stars of all the simulated clusters for random sampling (Fig. 3), constrained sampling (Fig. 4) and sorted sampling (Fig. 5), all with the physical limit $m_{\rm max*} = 150\,{\rm M}_\odot$.

As can be seen from Fig. 3, the random sample occupies the whole parameter space between the two extremes, which are either that nearly the whole cluster consists only of low-mass stars, or a single star accounts for the entire cluster mass ($m_{\rm max} = M_{\rm ecl}$). Such one-star clusters would correspond to freak star formation events such as is envisaged for a variable gas equation-of-state star formation theory (Li, Mac Low & Klessen 2005). For sorted sampling the clusters are shifted more towards smaller stellar masses and never touch this line. While the constrained sampling lies in between these two extremes and still populates the parameter space up to the identity relation.

Note that ${}^{l}\overline{m}^{\rm sort}_{\rm max}(M_{\rm ecl})$, shown in Figs 3–5 (thick dotted line in Fig. 5, and thin dotted line in Figs 3 and 4), is nearly identical to the semi-analytical estimate ${}^{l}m^{\rm ana}_{\rm max}(M_{\rm ecl})$ (equation 7, thick solid line in Figs 3–5). The slight deviations are probably due to the stochastic element in the process to decide which is the most massive star in the sorted Monte Carlo experiment (see Section 2.2.3).

The non-smoothness of the contour lines in the upper right-hand edge of the figures is an effect of low-number sampling. Here only the outermost contour line is present – indicating that there are only single events in this region of parameter space obtained with 2.5×10^7 clusters, which together have about 600×10^6 stars. This number of clusters comprises the computational limit of the available hardware.

The agreement between the mean value ${}^{l}\overline{m}^{\rm sort}_{\rm max}(M_{\rm ecl})$ and the semi-analytic result of Weidner & Kroupa (2004), ${}^{l}m^{\rm ana}_{\rm max}(M_{\rm ecl})$, is in

[2] For example, if $M_{\rm ecl} = 50\,{\rm M}_\odot$, $m_N = 10\,{\rm M}_\odot$ and $m_{N-1} = 5\,{\rm M}_\odot$, then for ${}^{*}M_{\rm ecl,ran} = 52\,{\rm M}_\odot$, $m_{\rm max}$ would be $10\,{\rm M}_\odot$, as 52 is closer to 50 than 42. If $M_{\rm ecl}$ would be $45\,{\rm M}_\odot$ then $m_{\rm max}$ would be $5\,{\rm M}_\odot$.

principle not surprising. The method of sorted adding of stellar masses in order to get the cluster mass corresponds to a Monte Carlo integration of equations (5) and (6). Therefore, the result should agree with the numerically integrated (semi-analytical) one.

Another difference between the samplings lies in the average mean stellar masses in the clusters. To determine these, cluster masses from 5 to $10^6\,\mathrm{M}_\odot$ are divided in 10 logarithmically equally spaced values and each is filled 10 000 times with stars from the IMF in the three different ways described in Sections 2.2.1, 2.2.2 and 2.2.3. The mean stellar mass for each cluster is calculated by

$$\overline{m} = \frac{1}{N}\sum_{N} m_\mathrm{i}, \tag{21}$$

where N is the number of stars in each cluster. Then for each cluster mass, $M_{\mathrm{ecl},j}(j = 1, \ldots, 10)$, the 'mean of means' is computed by

$$\overline{m}_j(M_{\mathrm{ecl},j}) = \frac{1}{N_\mathrm{ecl}}\sum_{N_\mathrm{ecl}} \overline{m_i}, \tag{22}$$

with $N_\mathrm{ecl} = 10\,000$.

The different average mean stellar masses are shown in Fig. 6. For the random sampling the mean is always about $0.36\,\mathrm{M}_\odot$, as expected for the canonical IMF between 0.01 and $150\,\mathrm{M}_\odot$. The other sampling methods have lower means for light clusters which rise up to $0.36\,\mathrm{M}_\odot$ for more-massive ones. This is a result of the limit which low-mass clusters impose on their stellar content. For random sampling only the number of stars determines the cluster mass, in contrast to reality where the natal cloud-mass and the star formation efficiency rule the final cluster mass.

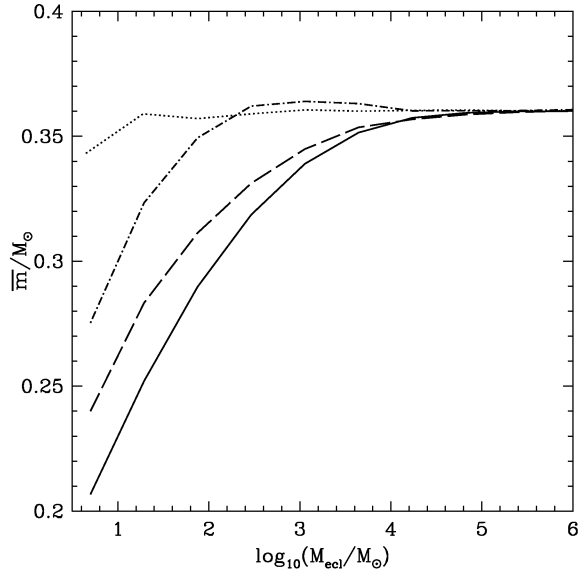

Figure 6. Average mean stellar mass for the different Monte Carlo samples against cluster mass (equation 22). For random sampling (dotted line) the value is constant within the numerical noise around the expected value of $0.36\,\mathrm{M}_\odot$. In the case of constrained sampling (dot–dashed line) and in the case of sorted sampling (long-dashed line) it starts rather low for low-mass clusters and rises up to the expected value of $0.36\,\mathrm{M}_\odot$. The solid line shows the relation described by equation (23). Note that the dashed line lies above the solid curve because the maximal stellar mass in the sorted-sampling algorithm is systematically higher than the analytical result (Figs 7–9 below) for cluster masses below $10^4\,\mathrm{M}_\odot$.

Also shown in Fig. 6 is the average mean stellar mass for the analytical model (equation 7), which is given by

$$\overline{m} = \frac{\int_{m_\mathrm{low}}^{m_\mathrm{max}(M_\mathrm{ecl})} m\xi\,\mathrm{d}m}{\int_{m_\mathrm{low}}^{m_\mathrm{max}(M_\mathrm{ecl})} \xi\,\mathrm{d}m}, \tag{23}$$

where $\xi(m)$ is equation (2).

2.2.5 *Comparison with observational data*

Table 1 shows a non-exhaustive compilation of cluster masses and upper stellar masses for a number of MW and LMC clusters (see Appendix A for more details). These data are shown as dots with error bars in Figs 7, 8 and 9. The result of a cluster formation simulation by Bonnell et al. (2003) is shown as a large triangle.

Fig. 7 compares the mean m_max values of the Monte Carlo experiments together with the observations from Table 1, the semi-analytical result of Weidner & Kroupa (2004) and the different results of the previous studies (Section 2.1). The 'unlimited' mean values are marked with a 'u', while the limited ones ($m_{\mathrm{max}*} = 150\,\mathrm{M}_\odot$) with an '$l$'. The mean values of the 'u' cases are all clearly distinct from the observations and not regarded further, while for the 'l' cases the mean values are in reasonable agreement with the observations. But especially ${}^{l,u}\overline{m}^{\mathrm{ran}}_{\mathrm{max}}(M_\mathrm{ecl})$ and ${}^{l,u}\overline{m}^{\mathrm{con}}_{\mathrm{max}}(M_\mathrm{ecl})$ lie above the observations, while ${}^{l}\overline{m}^{\mathrm{sort}}_{\mathrm{max}}(M_\mathrm{ecl})$ and ${}^{l}m^{\mathrm{ana}}_{\mathrm{max}}(M_\mathrm{ecl})$ fit the observations rather well.

The observational analysis (equations 8 and 9) by Larson (1982, 2003) and the analytical result (equation 10) of Elmegreen (1983) have a shallower slope and underestimate the observed stellar masses for $M_\mathrm{ecl} > 100\,\mathrm{M}_\odot$. The analytical result (equation 12) of Elmegreen (2000) and the star formation simulation (equation 13) by Bonnell et al. (2003, 2004) fit much better but ignore the observed upper mass limit for stars near $150\,\mathrm{M}_\odot$ (Weidner & Kroupa 2004; Figer 2005; Oey & Clarke 2005). Taking this into account leads to the semi-analytical (equation 7) relation. The Oey & Clarke (2005) expectation values for m_max(equation 14) follow quite well the constrained-sampling result, but in doing so they overpredict m_max in comparison with the observations.

In Fig. 8, only ${}^{u}\overline{m}^{\mathrm{con}}_{\mathrm{max}}(M_\mathrm{ecl})$ and ${}^{l}\overline{m}^{\mathrm{sort}}_{\mathrm{max}}(M_\mathrm{ecl})$ are shown but for different slopes of the IMF above $1\,\mathrm{M}_\odot$. For ${}^{u}\overline{m}^{\mathrm{con}}_{\mathrm{max}}(M_\mathrm{ecl})\alpha_3 = 2.35$, 2.70 and 3.00 is plotted, while for ${}^{l}\overline{m}^{\mathrm{sort}}_{\mathrm{max}}(M_\mathrm{ecl})$ the relations are plotted for $\alpha_3 = 2.35$ and 2.70. In the case of ${}^{u}\overline{m}^{\mathrm{con}}_{\mathrm{max}}(M_\mathrm{ecl})$ we can see that the steeper IMF slopes fit the observations much better. Therefore, if Sagar & Richtler (1991) are right about their notion that unresolved binaries would mask a steep underlying IMF, constrained or even random sampling cannot be ruled out. But it should be noted here, that the Sagar & Richtler (1991) examination was only carried out for stars with masses between 2 and $14\,\mathrm{M}_\odot$. Therefore, the O-star regime has not yet been explored in this respect.

2.3 Ageing of the stars

To see if stellar evolution together with constrained sampling can mimic the effect of the sorted sampling, stars with $m \leqslant 50\,\mathrm{M}_\odot$ are evolved with the single stellar evolution (SSE) package from Hurley, Pols & Tout (2000), while for more-massive stars fitting formulae derived from stellar evolution models computed by Schaller et al. (1992) are used (see Appendix B for for the detailed fitting functions). For this purpose 1×10^7 clusters are chosen from an ECMF with $\beta = 2.35$ and then aged for 1, 2, 2.5, 3 and 3.5 Myr. The evolved stellar masses are added after excluding neutron stars and

Table 1. Empirical cluster masses, maximal star masses within these clusters and cluster ages from the literature.

Designation	$M_{\rm ecl}$ ($\rm M_\odot$)	$m_{\rm maxobs}$ ($\rm M_\odot$)	Age (Myr)	Source
Taurus–Auriga	25 ± 15	2.2 ± 0.2	1–2	(1)
Ser SVS2	30 ± 15	2.2 ± 0.2	2	(2)
NGC 1333	80 ± 30	5 ± 1.0	1–3	(3)
ρ Oph	100 ± 50	8 ± 1.0	0.1–1	(4)
IC 348	109 ± 20	6 ± 1.0	1.3	(5)
NGC 2024	225 ± 30	20 ± 4	0.5	(6)
σ Ori	225 ± 30	20 ± 4	2.5	(6)
Mon R2	259 ± 60	10 ± 1	0–3	(7)
NGC 2264	355 ± 50	25 ± 5	3.1	(8)
NGC 6530	815 ± 115	20 ± 4	2.3	(9)
Ber 86	1500 ± 500	40 ± 8	2–3	(10)
M42	2200 ± 300	45 ± 5	<1	(11)
NGC 2244	6240 ± 124	70 ± 14	1.9	(12)
NGC 6611	$2 \times 10^4 \pm 10\,000$	85 ± 15	1.3 ± 0.3	(13)
Tr 14/16	$4.3 \times 10^4 -2.3 \times 10^4/+2 \times 10^4$	120 ± 15	<3	(14)
Arches	$5 \times 10^4 -3.5 \times 10^4/+2 \times 10^4$	135 ± 15	2.5	(15)
R136	$1 \times 10^5 -5 \times 10^4/+1.5 \times 10^5$	145 ± 10	1–2	(16)
Simulation	580	27	0.456	(17)

(1): Briceño et al. (2002); (2): Kaas et al. (2004); (3): Aspin (2003), Getman et al. (2002); (4): Wilking, Lada & Young (1989); Larson (2003); (5) Preibisch & Zinnecker (2001), Lada & Lada (2003); (6) Sherry, Walter & Wolk (2004); (7): Carpenter et al. (1997); (8): Sung, Bessell & Chun (2004); (9): Prisinzano et al. (2005), Damiani et al. (2004); (10): Massey, Johnson & DeGioia-Eastwood (1995); Vallenari et al. (1999); (11): Hillenbrand & Hartmann (1998), Hillenbrand et al. (1998); (11): Massey et al. (1995), Park & Sung (2002); (13): Bonatto, Santos & Bica (2005); (14): Massey & Johnson (1993), Massey et al. (1995); (15): Figer et al. (2002); (16): Massey & Hunter (1998), Selman et al. (1999); and (17): Bonnell et al. (2003)

.

black holes to give $M_{\rm ecl}$ and then searched for the most massive star in each cluster.

In Fig. 9, the effect of this ageing is shown. Within the first 2.5 Myr the mean values of the sorted-sampling and the constrained-sampling algorithms are clearly distinct. The lines change due to mass loss of the heavy stars, which amounts to about 40 to 50 per cent of the initial stellar mass, according to the models used (see Appendix C for a comparison of different models). After 2.5 Myr the massive stars start to explode as supernovae and the constrained-sampled clusters $[{}^{l}\overline{m}^{\rm con}_{\rm max}(M_{\rm ecl})]$ move closer to the sorted-sampled ones $[{}^{l}\overline{m}^{\rm sort}_{\rm max}(M_{\rm ecl})]$ for $M_{\rm ecl} \geqslant 10^3\,\rm M_\odot$. After 1 Myr and for clusters with $M_{\rm ecl} \geqslant 10^3\,\rm M_\odot$, ageing shifts ${}^{l}\overline{m}^{\rm con}_{\rm max}(M_{\rm ecl})$ closer to the observations, making the distinction between constrained and sorted sampling impossible. Nevertheless, the observational data for $M_{\rm ecl} < 10^3\,\rm M_\odot$ agree much better with sorted than with constrained sampling for all ages.

It must be noted here that the observed stellar masses ($m_{\rm maxobs}$) in Table 1 are a mixture of present-day (PD) masses and zero-age main-sequence (ZAMS) masses. For stars below, roughly, $50\,\rm M_\odot$ this is not critical, as for them mass loss is not dominant during the first 3 Myr. However, the three most massive clusters have ZAMS maximal stellar masses and therefore cannot be compared with the aged tracks in Fig. 9. Our previous (Section 2.2) comparison of the data with ZAMS isochrones is thus justified.

2.4 Statistical analysis

In order to evaluate the statistical significance of the differences between the Monte Carlo simulations and the observations, two statistical tests are applied. The statistical tests are only applied to the zero-age Monte Carlo samples, as the PD and ZAMS masses for low-mass stars do not differ substantially for such young clusters and all the massive stars ($m \geqslant 50\,\rm M_\odot$) in the observational sample are always ZAMS masses. While for ages $\leqslant 2.5$ Myr different stellar models agree rather reasonably on the properties and evolution of massive stars (see Appendix C for a substantial comparison of some models) the theoretical foundation of the formation of such massive stars is still very weak (for a detailed discussion of massive stars, see Kroupa & Weidner 2005).

The probabilities that the observed masses of the most massive stars, $m_{\rm maxobs}$, in the clusters are drawn from the three different Monte Carlo samples are calculated. In order to do so, the distribution of $m_{\rm max}$ around each observed cluster mass, $\mu\,(m_{\rm max} : M_{\rm ecl})$, is examined for the three samplings, whereby we only use those that have a maximal stellar mass, $m_{\rm max*} = 150\,\rm M_\odot$. If the mean value, $\overline{m}_{\rm max}(M_{\rm ecl})$, of the Monte Carlo distribution, $\mu(m_{\rm max})$, for a cluster mass is higher than the observed maximal mass, $m_{\rm maxobs}$, then the distribution is integrated from the lower limit, $m_{\rm low}$, to $m_{\rm maxobs}$ and divided by the integral from $m_{\rm low}$ to ${}^{l}\overline{m}^{\rm ran,\,con,\,sort}_{\rm max}$,

$$P(m_{\rm max} \leqslant m_{\rm maxobs}) = \frac{\int_{m_{\rm low}}^{m_{\rm maxobs}} \mu\ {\rm d}m}{\int_{m_{\rm low}}^{{}^{l}\overline{m}^{\rm ran,\,con,\,sort}_{\rm max}} \mu\ {\rm d}m}. \qquad (24)$$

This is the probability of observing a maximum mass $m_{\rm max}$ as small as or smaller than $m_{\rm maxobs}$.

If, on the other hand, the mean value is smaller than $m_{\rm maxobs}$, the integral is taken from $m_{\rm maxobs}$ to the upper mass limit, $m_{\rm max*}$, and is divided by the integral from the mean value, ${}^{l}\overline{m}^{\rm ran,\,con,\,sort}_{\rm max}$, to $m_{\rm max*}$,

$$P(m_{\rm max} \geqslant m_{\rm maxobs}) = \frac{\int_{m_{\rm maxobs}}^{m_{\rm max*}} \mu\ {\rm d}m}{\int_{{}^{l}\overline{m}^{\rm ran,\,con,\,sort}_{\rm max}}^{m_{\rm max*}} \mu\ {\rm d}m}. \qquad (25)$$

This is the probability of observing an $m_{\rm max}$ as large as or larger than $m_{\rm maxobs}$. Together, equations (24) and (25) are the probability of

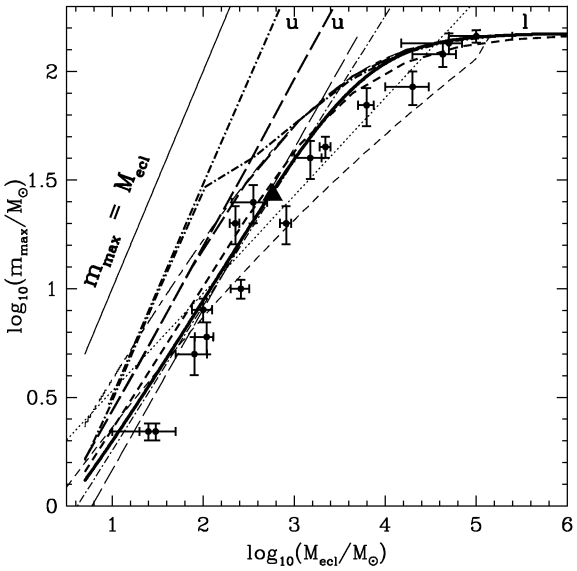

Figure 7. The thick solid line shows the dependence of the maximal star mass on the cluster mass for $\alpha_3 = 2.35$ from the semi-analytical model [$^{l}m^{\rm ana}_{\rm max}(M_{\rm ecl})$, equation 7]. The thick short-dashed line shows the mean maximum stellar mass for sorted sampling [$^{l}\overline{m}^{\rm sort}_{\rm max}(M_{\rm ecl})$, see Section 2.2.3]. The long-dashed lines are mass-constrained random-sampling [$^{l,u}\overline{m}^{\rm con}_{\rm max}(M_{\rm ecl})$, see Section 2.2.2] results with an upper mass limit of $10^6\,{\rm M}_\odot$ (straight line) and $150\,{\rm M}_\odot$ (curved line). Pure random-sampling models [$^{l,u}\overline{m}^{\rm ran}_{\rm max}(M_{\rm ecl})$, see Section 2.2.1] are printed as dot–dashed lines. The curved one is sampled to $m_{\rm max} = 150\,{\rm M}_\odot$ while the straight one assumes $m_{\rm max*} = 10^6\,{\rm M}_\odot$. The thin solid line shows the identity relation, were a 'cluster' consists of only one star. The dots with error bars are observed clusters (see Table 1), while the triangle is a result from a star formation simulation (equation 13) with an SPH code (Bonnell et al. 2003). A previous study of massive stars in clusters (equation 8 and 9) by Larson (1982, 2003) is shown as a thin dotted line, while an analytic estimate (equation 10) by Elmegreen (1983) as a thin short-dashed line and equation (12) by Elmegreen (2000) as a thin long-dashed line. The thin long-dashed–short-dashed line marks the expectation values (equation 14) from Oey & Clarke (2005).

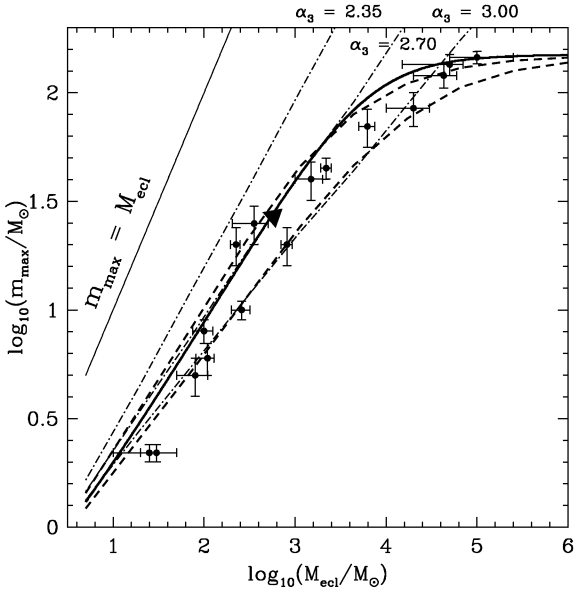

Figure 8. The thick solid line shows $^{l}m^{\rm ana}_{\rm max}\,(M_{\rm ecl})$ for $\alpha_3 = 2.35$ (equation 7). The thick dashed lines are $^{l}\overline{m}^{\rm sort}_{\rm max}(M_{\rm ecl})$ for $\alpha_3 = 2.35$ (upper line) and 2.70 (lower line). The dot–dashed lines are constrained-sampling Monte Carlo results, $^{u}\overline{m}^{\rm con}_{\rm max}(M_{\rm ecl})$, with three different slopes ($\alpha_3 = 2.35$, 2.70 and 3.00 above $1\,{\rm M}_\odot$) of the input stellar IMF. The thin solid line shows the identity relation. The dots with error bars are observed clusters (Table 1), while the triangle is a result from the star formation simulation with an SPH code (Bonnell et al. 2003).

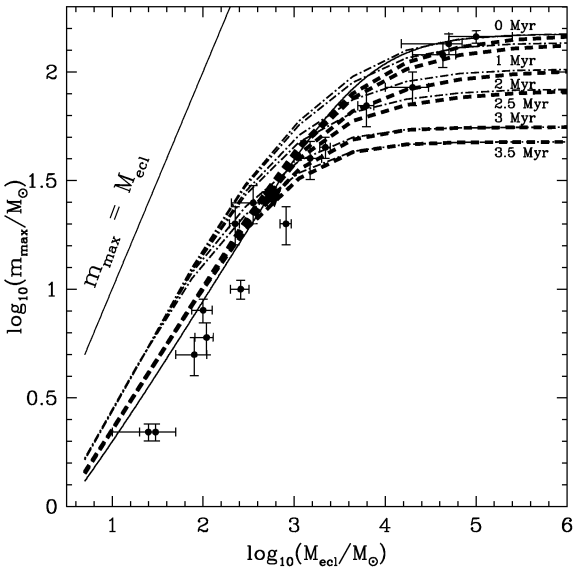

Figure 9. As Fig. 7 but the mean curves include ageing by 1, 2, 2.5, 3 and 3.5 Myr. The stars in the Monte Carlo simulations are subject to stellar evolution according to the SSE package by Hurley et al. (2000) and our own extensions for stars $\geqslant 50\,{\rm M}_\odot$ which includes not only finite lifetimes but also stellar mass loss. The thick dashed lines are for clusters which are constructed using sorted sampling, while the dot–dashed lines are for constrained sampling. Note that $^{l}\overline{m}^{\rm con}_{\rm max}(M_{\rm ecl}) = {}^{l}\overline{m}^{\rm sort}_{\rm max}(M_{\rm ecl})$ for ages $\gtrsim$3 Myr and $M_{\rm ecl} \geqslant 10^3\,{\rm M}_\odot$.

observing an $m_{\rm maxobs}$ such that $|m_{\rm maxobs} - \overline{m}_{\rm max}(M_{\rm ecl})| \geqslant |m_{\rm max} - \overline{m}_{\rm max}(M_{\rm ecl})|$. Figs 10 and 11 show a schematic view of this integration process by means of two examples (Taurus–Auriga and NGC 2264) for all three cases of sampling.

The resulting combined probabilities (Π in Table 2, acquired by multiplying the individual probabilities) for all clusters are 10^{-9} for random sampling, 10^{-6} for constrained sampling and 10^{-4} for sorted sampling, with the highest probability thus being attained for sorted sampling. Table 2 shows the individual probabilities P for each $m_{\rm maxobs}$.

To obtain a completely different statistic on the correspondence between data and theory, we also apply a Wilcoxon signed-rank test (Bhattacharyya & Johnson 1977) to determine how significant the differences between the data and the $^{l}\overline{m}^{\rm ran,\,con,\,sort}_{\rm max}$ relations are. For this test the differences of the data points and the mean values are calculated,

$$\Delta m_j = m_{{\rm maxobs},\,j} - {}^{l}\overline{m}^{\rm ran,\,con,\,sort}_{{\rm max},\,j}\,(\text{for a given } M_{{\rm ecl},\,j}), \qquad (26)$$

and then ranked according to their absolute value. Afterwards, only the positive-signed ranks are added and this sum is then cross-checked with tabulated values (Bhattacharyya & Johnson 1977) in order to get the probability P that the null hypothesis (data points and the $^{l}\overline{m}^{\rm ran,\,con,\,sort}_{\rm max}$ relations are the same within the uncertainties) is true. In the case of random sampling (Section 2.2.1) and constrained sampling (Section 2.2.2) $P = 0.000\,14$, while $P = 0.0458$ for sorted sampling (Section 2.2.3).

Thus, both tests taken together suggest strongly that sorted-sampling best describes the empirical data. The physical interpretation of this result is discussed in Section 4.

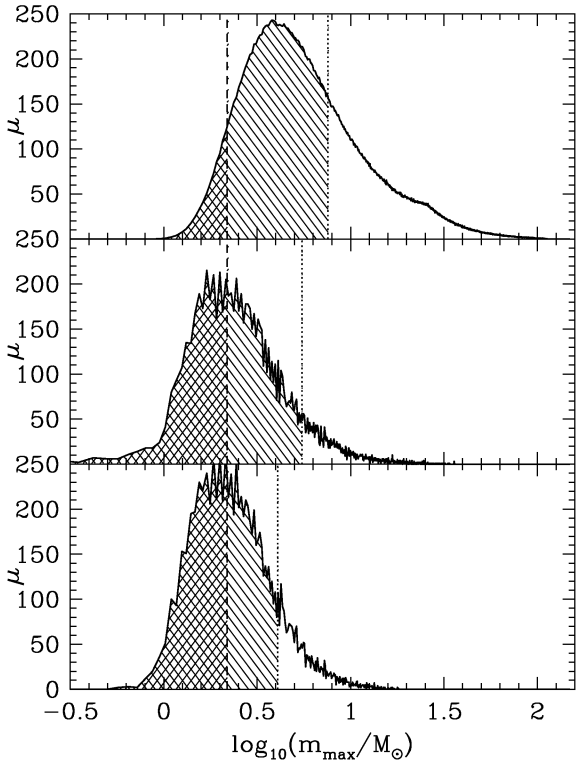

Figure 10. All panels: vertical slice through Figs 3, 4 and 5 at $M_{\rm ecl} = 25\,{\rm M}_\odot$ (Taurus–Auriga). The vertical axis plots the number of clusters μ which have the maximal mass $m_{\rm max}$ in a logarithmic bin $\Delta\log_{10} m_{\rm max} = 0.01044$. Top panel: histogram of the number of clusters for the random-sampling models (Section 2.2.1). The vertical dashed line marks the observed upper mass in Taurus–Auriga, while the dotted line is the mean (or expectation) value of the Monte Carlo experiment, ${}^{l}\overline{m}^{\rm ran}_{\rm max}(M_{\rm ecl})$. The probability of observing an $m_{\rm max}$ as small as or smaller than $m_{\rm maxobs}$ is $P(m_{\rm max} \leqslant m_{\rm maxobs})$ which is the area under the curve left-hand side of the dashed line divided by the area under the curve left-hand side of the dotted line. Middle panel: like top panel but for the constrained-sampling Monte Carlo experiment (Section 2.2.2). Bottom panel: as top panel but in this case for sorted sampling (Section 2.2.3). All panels: note that the areas to the left-hand and right-hand sides of the mean value do not appear equal because the binning was done linearly but is plotted on a logarithmic scale.

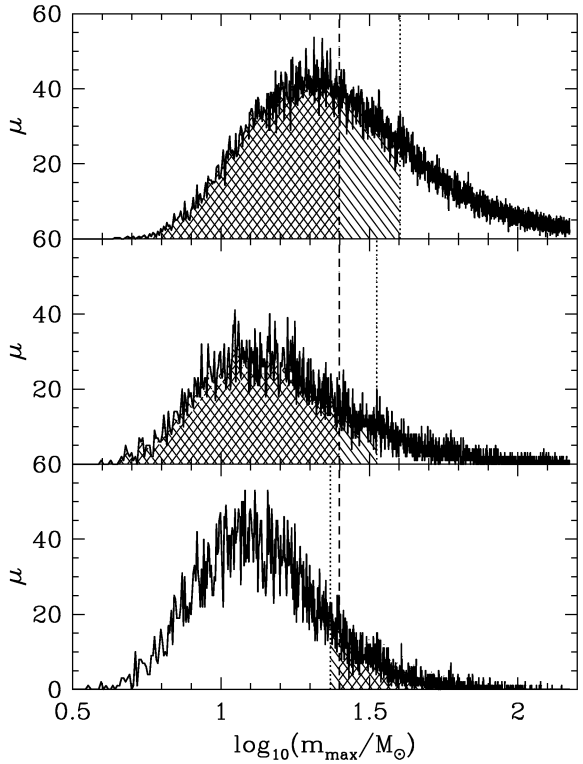

Figure 11. All three panels like Fig. 10 but in this case for a cluster mass of $355\,{\rm M}_\odot$ (NGC 2264). For the sorted sampling (bottom panel) the mean is lower than the observed value of $m_{\rm max}$. Therefore, the probability is calculated by dividing the area to the right-hand side of the observed value (dashed line) through the area to the right-hand side of the expectation value (dotted line).

3 THE MONTE CARLO SIMULATIONS OF THE INTEGRATED GALAXIAL STELLAR IMF

We have thus seen that the observational data strongly favour a particular $m_{\rm max}(M_{\rm ecl})$ relation, namely, the ${}^{l}\overline{m}^{\rm sort}_{\rm max} \approx {}^{l}m^{\rm ana}_{\rm max}$ relation. This has profound implications for composite stellar populations.

Fig. 12 shows the result of the semi-analytic approach by Kroupa & Weidner (2003) assuming $\beta = 2.35$ for the ECMF. The stellar IMF in each cluster has, in all cases, the standard or canonical three-part power-law form (equation 2). For the minimum 'cluster' mass, $M_{\rm ecl,min} = 5\,{\rm M}_\odot$ (a dozen stars), and for the maximal cluster mass, $M_{\rm ecl,max} = 10^6\,{\rm M}_\odot$, are used. The power-law index $\alpha_{\rm IGIMF}$ of the resulting semi-analytical IGIMF is well approximated by $\alpha_{\rm IGIMF} = 3.00$ for $m \gtrsim 1\,{\rm M}_\odot$. In Kroupa & Weidner (2003), we already noted that this is probably the reason why the Galactic field IMF deduced by Scalo (1986) ($\alpha_3 \approx 2.7$) is steeper than the canonical stellar IMF.

We now apply the Monte Carlo experiments introduced above to the computation of the IGIMF (equation 4). The resulting IGIMF is constructed by mass-binning all stars in all clusters. It is shown as a long-dashed line in Fig. 13 for constrained sampling and as a short-dashed line for sorted sampling. Additionally, the 'input' standard stellar IMF (solid line) and the semi-analytical IGIMF from Fig. 12 (dotted line) are shown. The IGIMF obtained with sorted sampling agrees very well with the semi-analytical result, while the IGIMF obtained from constrained sampling shows a flatter slope. Even this IGIMF nevertheless differs strongly from the standard IMF with a Salpeter slope, as a result of the imposed condition of a given cluster mass.

3.1 Different ECMF

Following-on from our discussion in Weidner & Kroupa (2005) we explore how a different ECMF affects the IGIMF. Any ECMF with $\beta > 2.35$ will increase the steepening of the IGIMF. However, below 50 or 100 $\,{\rm M}_\odot$ (approximately) the ECMF is poorly defined observationally (Lada & Lada 2003), and we consider here the implication of a flatter ECMF at low masses while keeping $\beta = 2.35$ for $M_{\rm ecl} > 50$ or $100\,{\rm M}_\odot$.

In Fig. 14, we explore the effect of a different ECMF than our standard assumption ($\beta = 2.35$ over the whole range of cluster masses). This figure is the same as Fig. 13, but the constrained-sampling and sorted-sampling results for two EMCFs with $\beta_1 = 1$ for clusters below 50 and $100\,{\rm M}_\odot$, and $\beta_2 = 2.35$ for clusters above these masses, are shown as dotted and dashed lines, respectively. The steeper ones show the sorted-sampling cases. The change of the ECMF reduces the effect of the ECMF on the IGIMF but is still clearly visible, giving $\alpha_{\rm IGIMF,con} = 2.56$, $\alpha_{\rm IGIMF,sort} = 2.88$

Table 2. Probabilities that the $m_{\rm maxobs}$ are from one of the three Monte Carlo samples.

Cluster	Random sampling (per cent)	Constrained sampling (per cent)	Sorted sampling (per cent)
Taurus–Auriga	25.0	36.2	45.4
Ser SVS2	12.5	33.1	41.5
NGC 1333	24.7	29.4	41.1
ρ Oph	31.5	60.6	81.7
IC 348	9.2	38.2	52.5
NGC 2024	69.1	86.0	76.4
σ Ori	69.1	86.0	76.4
Mon R2	25.8	27.1	37.5
NGC 2264	57.6	81.9	84.7
NGC 6530	27.2	32.4	44.3
Ber 86	39.3	53.9	76.3
M42	43.9	53.6	75.5
NGC 2244	34.1	40.4	68.0
NGC 6611	6.4	5.6	32.2
Tr 14/16	42.4	44.8	96.6
Arches	75.0	88.2	67.4
R136	65.7	82.3	42.2
Π	3.37×10^{-9}	9.22×10^{-7}	9.18×10^{-5}

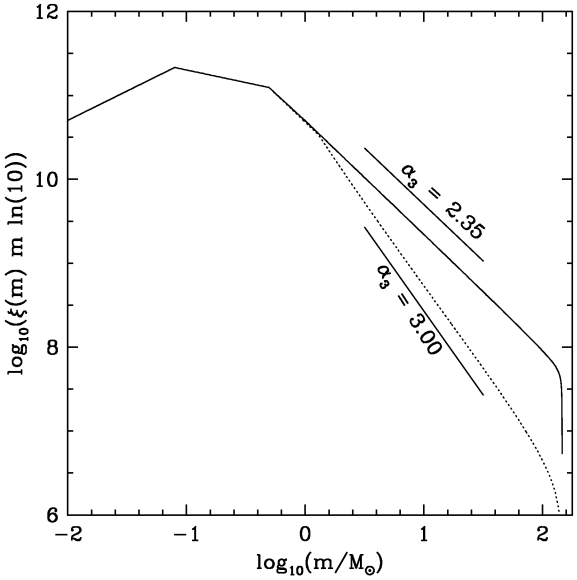

Figure 12. Solid line: canonical stellar IMF, $\xi(m)$, in logarithmic units and given by the standard three-part power-law form (equation 2), which has $\alpha_3 = 2.35$ for $m > 0.5\,{\rm M}_\odot$. Dotted line: semi-analytical $\xi_{\rm IGIMF}(m)$ for $\beta = 2.35$. The IMFs are scaled to have the same number of objects in the mass interval 0.01–1.0 $\rm M_\odot$. Note the turn-down near $m_{\rm max*} = 150\,{\rm M}_\odot$ which comes from taking the fundamental upper mass limit explicitly into account (Weidner & Kroupa 2004). Two lines with slopes $\alpha_{\rm line} = 2.35$ and 3.00 are indicated.

for $\beta = 1$ ($M_{\rm ecl} < 50\,{\rm M}_\odot$) and $\alpha_{\rm IGIMF,con} = 2.52$, $\alpha_{\rm IGIMF,sort} = 2.86$ for $\beta = 1$ for ($M_{\rm ecl} < 100\,{\rm M}_\odot$), as opposed to our standard assumption for which $\alpha_{\rm IGIMF,con} = 2.8$ and $\alpha_{\rm IGIMF,sort} = 3.0$.

4 DISCUSSION AND CONCLUSIONS

In this contribution a number of Monte Carlo experiments are conducted in order to constrain the relation between the maximal mass a star can have in a cluster and the mass of the cluster, and to further study the IMF of composite populations, that is, the integrated galaxial IMF.

We consider the following three possible ways of forming clusters.

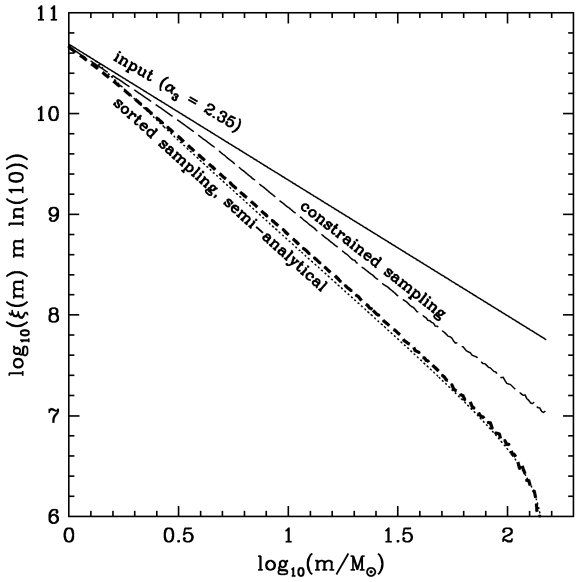

Figure 13. Solid line: standard stellar IMF with $\alpha_3 = 2.35$ for $m > 1\,{\rm M}_\odot$ (same as in Fig. 12). Dotted line: IGIMF resulting from the semi-analytical approach with $\beta = 2.35$ (as in Fig. 12). Short-dashed line: IGIMF obtained from sorted sampling. Long-dashed line: IGIMF produced by constrained sampling of stars. As the IMF below 1 $\rm M_\odot$ does not change, only the region above 1 $\rm M_\odot$ is plotted here.

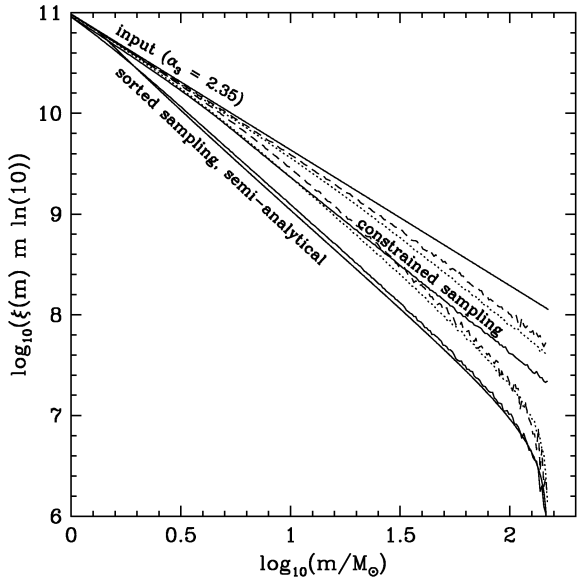

Figure 14. As Fig. 13 (all lines from Fig. 13 are solid) but in addition the results for two different ECMFs are plotted as dotted and dashed lines. In the dotted case the slope of the ECMF is $\beta_1 = 1$ for clusters below $50\,{\rm M}_\odot$. In the dashed case $\beta_1 = 1$ below $100\,{\rm M}_\odot$. In both the cases $\beta_2 = 2.35$ for clusters above these limits. As the IMF below 1 $\rm M_\odot$ does not change, only the region above 1 $\rm M_\odot$ is shown. The respective models assuming sorted sampling are always steeper than those assuming constrained sampling.

(i) Completely randomly. Clusters are filled randomly with stars and then their masses, $M_{\rm ecl}$, are calculated (random sampling).

(ii) Cluster-masses are picked from an ECMF and used as a constraint in constructing the stellar content of each cluster (constrained sampling).

(iii) Cluster-masses are picked from an ECMF, and the clusters are then filled with stars by randomly selecting from the canonical IMF, sorting the stellar masses in ascending order and constraining their sum to be the cluster mass (sorted sampling).

In all the cases (i–iii), the most massive star, $m_{\rm max}$, in each cluster is found, and the average or expectation value, $\overline{m}_{\rm max}$, is calculated for the ensemble of clusters near $M_{\rm ecl}$ to give the relations ${}^{l,u}\overline{m}^{\rm ran,\,con,\,sort}_{\rm max}(M_{\rm ecl})$, where '$l$ and u' refer to models with or without a physical stellar mass limit of 150 $\rm M_\odot$.

The most important and surprising result is that the sorted-sampling algorithm best represents the observational data of young ($\leqslant$3 Myr) clusters. Constrained and random sampling do not fit the observations.

That our sorted-sampling algorithm for making stars fits the observational maximal stellar mass–star cluster mass data so well would appear to imply that clusters form in an *organized fashion*. The physical interpretation of the algorithm (i.e. of the Monte Carlo integration) is that as a pre-cluster core contracts under self-gravity the gas densities increase and local density fluctuations in the turbulent medium lead to low-mass star formation, perhaps similar to what is seen in Taurus–Auriga. As the contraction proceeds and before feedback from young stars begins to disrupt the cloud, star formation activity increases in further density fluctuations with larger amplitudes thereby forming more-massive stars. The process stops when the most massive stars that have just formed supply sufficient feedback energy to disrupt the cloud (Elmegreen 1983). Thus, less-massive pre-cluster cloud-cores would 'die' at a lower maximum stellar mass than more-massive cores. But in all cases stellar masses are limited by the physical maximum mass, $m \leqslant m_{\rm max}(M_{\rm ecl}) \leqslant m_{\rm max*}$. This scenario is nicely consistent with the hydrodynamic cluster formation calculations presented by Bonnell et al. (2003) and Bonnell et al. (2004). We note here that Bonnell et al. (2004) found their theoretical clusters to form hierarchically from smaller subclusters, and together with continued competitive accretion this leads to the relation $m_{\rm max} \propto M_{\rm ecl}^{2/3}$ (equation 13) in excellent agreement with our compilation of observational data for clusters with masses below $M_{\rm ecl} = 4000\,\rm M_\odot$. While this agreement is stunning, the detailed outcome of the currently available SPH modelling in terms of stellar multiplicities is not right (Goodwin & Kroupa 2005), and feedback that ultimately dominates the process of star formation, given the generally low star formation efficiencies observed in cluster-forming volumes (Lada & Lada 2003), is not yet incorporated in the modelling.

Stellar evolution is the major caveat here. But the comparison of different models (see Appendix C) shows a general agreement of the lifetimes and relevant parameters (mass, $\rm T_{eff}$ and luminosity) for the models considered here. Therefore, not different models but an intrinsically steeper IMF ($\alpha_3 \gtrsim 2.8$) could shift the expectation values for random and constrained sampling into the observed regime. Such a steep IMF may be possible if it is masked by unresolved multiple stars, something we are investigating now.

Furthermore, the Monte Carlo experiments ascertain the results of Kroupa & Weidner (2003) and Weidner & Kroupa (2005) regarding the steep IGIMF, especially so if sorted sampling is used. In the constrained-sampling case the IGIMF slope is still steeper than the input IMF but less steep than with sorted sampling. But it should be noted here that a very recent result by Elmegreen & Scalo (2006) shows that it is also possible to interpret present-day mass function (PDMF) variations falsely, as IMF variations when the SFR is assumed to be constant when in reality being burst-like. This result has not yet been implemented in our description of the IGIMF.

In summary we conclude the following.

(i) There exists a well-defined relation, $m_{\rm max} = m_{\rm max}(M_{\rm ecl})$, between the most massive star in a cluster and the cluster mass. The conjecture that a cluster consists of stars randomly picked from an invariant IMF between 0.01 and 150 $\rm M_\odot$ would therefore appear to be wrong.

(ii) Star clusters appear to form in an ordered fashion, starting with the lowest-mass stars until feedback is able to outweigh the gravitationally induced formation process.

(iii) IGIMFs must *always* be steeper for $m > 1\,\rm M_\odot$ than the stellar IMF that results from a local star formation event.

It will be important to further test the results presented here on the $m_{\rm max}(M_{\rm ecl})$ relation by compiling larger observational samples of young clusters. As this contribution has shown, it appears that the $m_{\rm max}(M_{\rm ecl})$ relation would be rather fundamental to galactic and extragalactic astrophysics.

ACKNOWLEDGMENTS

We are very thankful to Jarrod R. Hurley for kindly providing us with his very useful SSE software package, and to Simon P. Goodwin and Jan Pflamm for useful discussions. This research has been supported by DFG grant KR1635/3.

REFERENCES

Aspin C., 2003, AJ, 125, 1480
Bell E. F., McIntosh D. H., Katz N., Weinberg M. D., 2003, ApJS, 149, 289
Bhattacharyya G. K., Johnson R. A., 1977, Statistical Concepts and Methods. Wiley, New York
Bonatto C., Santos J. F. C. Jr., Bica E., 2005, A&A, preprint (astro-ph/0509805)
Bonnell I. A., Bate M. R., Vine S. G., 2003, MNRAS, 343, 413
Bonnell I. A., Vine S. G., Bate M. R., 2004, MNRAS, 349, 735
Briceño C., Luhman K. L., Hartmann L., Stauffer J. R., Kirkpatrick J. D., 2002, ApJ, 580, 317
Carpenter J. M., Meyer M. R., Dougados C., Strom S. E., Hillenbrand L. A., 1997, AJ, 114, 198
Cox A. N., 2000, in Cox A. N., ed., Allen's Astrophysical Quantities, 4th edn. Springer, New York
Damiani F., Flaccomio E., Micela G., Sciortino S., Harnden F. R. Jr., Murray S. S., 2004, ApJ, 608, 781
Elmegreen B. G., 1983, MNRAS, 203, 1011
Elmegreen B. G., 1999, in Beckman J. E., Mahoney T. J., eds, ASP Conf. Ser. Vol. 187, The Evolution of Galaxies on Cosmological Timescales. Astron. Soc. Pac., San Francisco, p. 145
Elmegreen B. G., 2000, ApJ, 539, 342
Elmegreen B. G., 2005, in Richard de Grijs and Rosa M. Gonzalez Delgado, eds, ASSL Vol. 329, Starbursts: from 30 Doradus to Lyman Break Galaxies. Springer, Dordrecht, p. 57
Elmegreen B. G., Scalo J. M., 2006, ApJ, 636, in press (astro-ph/0509282)
Figer D. F., 2005, Nat, 434, 192
Figer D. F., Najarro F., Gilemore D. et al., 2002, ApJ, 581, 258
Getman K. V., Feigelson E. D., Townsley L., Bally J., Lada C. J., Reipurth B., 2002, ApJ, 575, 354
Gieles M., Larsen S. S., Bastian N. J., Stein I. T., A&A, submitted
Goodwin S. P., Kroupa P., 2005, A&A, 439, 565
Hillenbrand L. A., Hartmann L. W., 1998, ApJ, 492, 540

Hillenbrand L. A., Strom S. E., Calvet N., Merrill K. M., Gotley I., Makidon R. B., Meyer M. R., Skrutsie M. F., 1998, AJ, 116, 1816
Hunter D. A., Elmegreen B. G., Dupuy T. J., Mortonson M., 2003, AJ, 126, 1836
Hurley R. H., Pols O. R., Tout C. A., 2000, MNRAS, 315, 543
Kaas A. A. et al., 2004, A&A, 421, 623
Köppen J., Weidner C., Kroupa P. 2006, MNRAS, submitted
Kroupa P., 2001, MNRAS, 322, 231
Kroupa P., 2002, Sci, 295, 82
Kroupa P., Weidner C., 2003, ApJ, 598, 1076
Kroupa P., Weidner C., 2005, in Cesaroni R., Churchwell E., Felli M., Walmsley C. M., eds, IAU Symp. 227, Massive Star Birth: A Crossroads of Astrophysics. Cambridge Univ. Press, Cambridge, p. 423
Kroupa P., Tout C. A., Gilmore G., 1993, MNRAS, 262, 545
Lada C. J., Lada E. A., 2003, ARAA, 41, 57
Larson R. B., 1982, MNRAS, 200, 159
Larson R. B., 2003, in De Buizer J. M., van der Bliek N. S., eds, ASP Conf. Ser. Vol. 287, Galactic Star Formation Across the Stellar Mass Spectrum. Astron. Soc. Pac., San Francisco, p. 65
Li Y., Mac Low M.-M., Klessen R. S., 2005, ApJ, 620, 19
Massey P., 2002, ApJS, 141, 81
Massey P., 2003, ARA&A, 41, 15
Massey P., Hunter D. A., 1998, ApJ, 493, 180
Massey P., Johnson J., 1993, AJ, 105, 980
Massey P., Johnson K. E., DeGioia-Eastwood K., 1995, ApJ, 454, 151
Meynet G., Maeder A., 2003, A&A, 404, 975
Miller G., Scalo J. M., 1979, ApJS, 41, 513
Oey M. S., Clarke C. J., 2005, ApJ, 620, L430
Park B.-G., Sung H., 2002, AJ, 123, 892
Parker J. W., Zaritsky D., Stecher T. P., Harris J., Massey P., 2001, AJ, 121, 891
Piskunov A. E., Belikov A. N., Kharchenko N. V., Sagar R., Subramaniam A., 2004, MNRAS, 349, 1449
Preibisch T., Zinnecker H., 2001, AJ, 122, 866
Prisinzano L., Damiani F., Micela G., Sciortino S., 2005, A&A, 430, 941
Reid I. N., Gizis J. E., Hawley S. L., 2002, AJ, 124, 2721
Sagar R., Richtler T., 1991, A&A, 250, 324
Salpeter E. E., 1955, ApJ, 121, 161
Scalo J. M., 1986, Fundam. of Cosmic Phys., 11, 1
Scalo J. M., 1998, in Gilmore G., Howell D., eds, ASP Conf. Ser. Vol. 142, The Stellar Initial Mass Function (38th Herstmonceux Conference). Astron. Soc. Pac., San Francisco, p. 201
Scalo J. M., 2005, in Corbelli E., Palla F., Zinnecker H., eds, ASSL 327, IMF@50: The Initial Mass Function 50 Years Later. Springer, Dordrecht, p. 23
Schaller G., Schaerer D., Meynet G., Maeder A., 1992, A&AS, 96, 269
Selman F., Melnick J., Bosch G., Terlevich R., 1999, A&A, 347, 532
Sherry W. H., Walter F. M., Wolk S. J ., 2004, AJ, 128, 2316
Sirianni M., Nota A., De Marchi G., Leitherer C., Clampin M., 2000, ApJ, 533, 203
Sirianni M., Nota A., De Marchi G., Leitherer C., Clampin M., 2002, ApJ, 579, 275
Sung H., Bessell M. S., Chun M.-Y., 2004, AJ, 128, 1684
Vallenari A., Richichi A., Carraro G., Girardi L., 1999, A&A, 349, 825
Vanbeveren D., 1982 A&A, 115, 65
Weidner C., Kroupa P., 2004, MNRAS, 348, 187
Weidner C., Kroupa P., 2005, ApJ, 625, 754
Wilking B. A., Lada C.J., Young E. T., 1989, ApJ, 340, 823
Weidner C., Kroupa P., Larsen S. S., 2004, MNRAS, 350, 1503
Wyse R. F. G., Gilmore G., Houdashelt M. L., Feltzing S., Hebb L., Gallagher J. S. III, Smecker-Hane T. A., 2002, New Astron., 7, 395
Zhang Q., Fall S. M., 1999, ApJ, 527, L81

APPENDIX A: CLUSTER AND MAXIMAL STAR MASS DETERMINATION

The masses of the clusters in Table 1 are acquired as follows. In the case of NGC 1333, NGC 2024, NGC 6530, M42, ρ Ophiuchi, σ Orionis, Serpens SVS2, Arches and R136 the authors of the corresponding papers provide the required mass estimates. The masses for NGC 2244, NGC 2264, NGC 6611, IC 348, Monoceros R2, Taurus–Auriga, Berkley 86 and Trumpler 14/16 are calculated by determining the fraction (given as a percentage in Table A1) of observed stars in comparison with a canonical IMF from 0.01 $M_\odot$ up to the observed upper mass limit. With the fraction of all stars the total number of stars in the cluster is estimated by dividing the observed number of stars by the fraction. The total mass of the cluster, $M_{\rm ecl}$, is then calculated by multiplying the total number of stars with the mean stellar mass, $m_{\rm mean}$, for the canonical IMF from 0.01 $M_\odot$ to the observed upper mass limit. The relevant values are shown in Table A1.

For the maximal stellar masses in these clusters the values within these papers are used whenever possible, which is for NGC 2244, NGC 2264, NGC 6611, M42, ρ Ophiuchi, σ Orionis, Monoceros R2, Berkley 86, Trumpler 14/16, Arches and R136. In the other cases (NGC 1333, NGC 2024, NGC 6530, IC 348, Serpens SVS2 and Taurus–Auriga) mass estimates are derived from the spectral types of the most luminous members using the spectral-type mass relation from Cox (2000).

APPENDIX B: FITTING FORMULAE FOR MASSIVE STAR EVOLUTION

Because the Hurley et al. (2000) SSE package is only calibrated for stellar models up to 50 $M_\odot$, additional fitting formulae have been developed for more-massive stars. Based on the Schaller et al. (1992) models for 60, 85 and 120 $M_\odot$, functions for $m(t)$, $L(t)$ and $T_{\rm eff}(t)$ have been obtained:

Table A1. Observed mass ranges and the corresponding mean masses for those clusters for which we need to derive cluster masses.

Cluster	Number of stars observed	Per cent of all stars	Total number of stars	Mass range ($M_\odot$)	$m_{\rm mean}$ ($M_\odot$)	$M_{\rm ecl}$ ($M_\odot$)
Taurus–Auriga	100	92.8	108	0.02–2.2	0.236	25.5
IC 348	241	62.5	386	0.08–6.0	0.282	109
Mon R2	475	55.2	861	0.1–10.0	0.301	259
NGC 2264	600	55.3	1086	0.1–25.0	0.327	355
Ber 86	340	7.7	4421	0.8–40.0	0.338	1500
NGC 2244	400	2.2	17 937	2.0–70.0	0.348	6240
NGC 6611	362	0.6	56 563	5.0–85.0	0.352	20 000
Tr 14/16	768	0.6	120 000	5.0–120.0	0.357	43 000

B1 Mass evolution

As long as the age, t (in Myr), of the star is below $\tau_{\rm m}$, the main-sequence lifetime, the mass evolution can be described according to,

$$m(t) = m_{\rm ini}\, {\rm e}^{-(a_1\, t)^2}. \tag{B1}$$

For $\tau_{\rm m} < t \leqslant \tau_{\rm m} + {\rm d}t$

$$m(t) = -\frac{a_2}{{\rm d}t}\, t + b_1. \tag{B2}$$

For both the parameters are

$$\tau_{\rm m} = \frac{\left[{\rm e}^{-(m_{\rm ini}/t_{af})\, t_{am}}\right] + t_{ab}}{10^6},$$

$$a_1 = \frac{1}{\left(m_{aa}\, {\rm e}^{-m_{\rm ini}/m_{ab}}\right) + m_{ac}},$$

$$a_2 = m_{\rm ini}\,(1 - f_1),$$

$$f_1 = (f_m\, m_{\rm ini}) - f_b,$$

$$b_1 = a_2 \left(1 + \frac{1}{{\rm d}t} - \frac{\tau_{\rm m}}{a_2}\right),$$

and constants

$$m_{\rm aa} = 48.0,$$
$$m_{\rm ab} = 24.7,$$
$$m_{\rm ac} = 3.15,$$
$${\rm d}t = 0.42,$$
$$f_{\rm m} = 3.523\,808 \times 10^{-3},$$
$$f_{\rm b} = 6.190\,428 \times 10^{-3},$$
$$t_{\rm af} = 23.5,$$
$$t_{\rm am} = 1.25 \times 10^7,$$
$$t_{\rm ab} = 2.5 \times 10^6.$$

When t is larger than $\tau_{\rm m} + {\rm d}t$ the star is considered dead. No remnant mass, $T_{\rm eff}$ or luminosity is assigned.

The resulting curves for a 120-, 85-, 60- and 50 $-$ M$_\odot$ star (solid lines) in comparison with the model data (dotted lines) are plotted in Fig. B1.

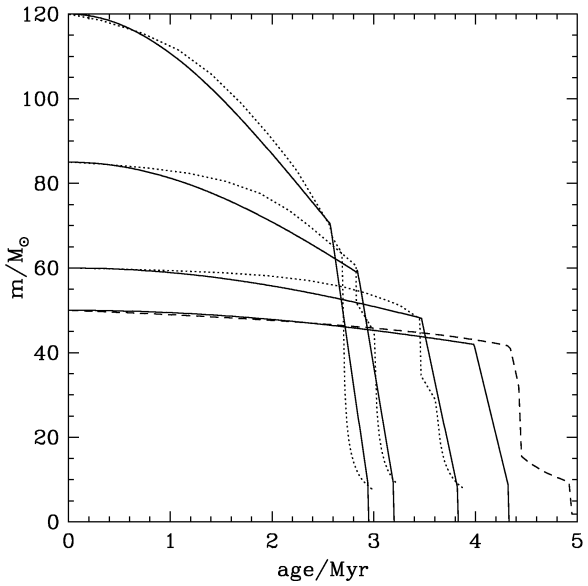

Figure B1. Stellar mass evolution for massive stars. The dotted lines are the Geneva models (Schaller et al. 1992), while the solid lines are the results from the fitting formulae described here. A Hurley et al. (2000) 50-M$_\odot$ star is shown as a dashed line.

B2 Effective temperature evolution

For $t \leqslant \tau_{\rm m}$ the equation

$$T_{\rm eff}(t) = T_{\rm eff,\,ini}\, {\rm e}^{(-t/a_3)^{b_2}}, \tag{B3}$$

adequately captures the evolution.

For $\tau_{\rm m} < t \leqslant \tau_{\rm m} + {\rm d}t$,

$$T_{\rm eff}(t) = f_2\, t + [T_{\rm low} - (f_2\, \tau_{\rm m})], \tag{B4}$$

is used.

The parameters are

$$T_{\rm eff,\,ini} = \begin{cases} T_{{\rm im}_1}\, m_{\rm ini} + T_{{\rm ib}_1} & m_{\rm ini} \geqslant 60\,{\rm M}_\odot, \\ T_{{\rm im}_2}\, m_{\rm ini} + T_{{\rm ib}_2} & m_{\rm ini} < 60\,{\rm M}_\odot, \end{cases}$$

$$a_3 = \begin{cases} tta_1 & m_{\rm ini} \geqslant 85\,{\rm M}_\odot, \\ tta_{2{\rm a}}\, m_{\rm ini} + tta_{2{\rm b}} & m_{\rm ini} < 85{\rm M}_\odot, \end{cases}$$

$$f_2 = \frac{(T_{\rm peak} - T_{\rm low})}{{\rm d}t},$$

$$T_{\rm low} = T_{\rm eff,\,ini}\, {\rm e}^{(-\tau_{\rm m}/a_3)^{b_2}},$$

and the constants

$$T_{{\rm im}_1} = 4.3 \times 10^{-3},$$
$$T_{{\rm ib}_1} = 4.425,$$
$$T_{{\rm im}_2} = 7.3333 \times 10^{-4},$$
$$T_{{\rm ib}_2} = 4.64,$$
$$b_2 = 2.3,$$
$$tta_1 = 9.0,$$
$$tta_{2{\rm a}} = -0.182\,857\,142,$$
$$tta_{2{\rm b}} = 24.542\,857\,19,$$
$$T_{\rm peak} = 4.8.$$

The resulting $T_{\rm eff}$ fitting curves are plotted in Fig. B2 for the same masses as in Fig. B1.

B3 Luminosity evolution

The luminosity evolution is divided into three parts. For $t \leqslant \tau_{\rm m}$,

$$L(t) = \left(\frac{L_{\rm jump} - L_{\rm ini}}{\tau_{\rm m}}\right) t + L_{\rm ini}. \tag{B5}$$

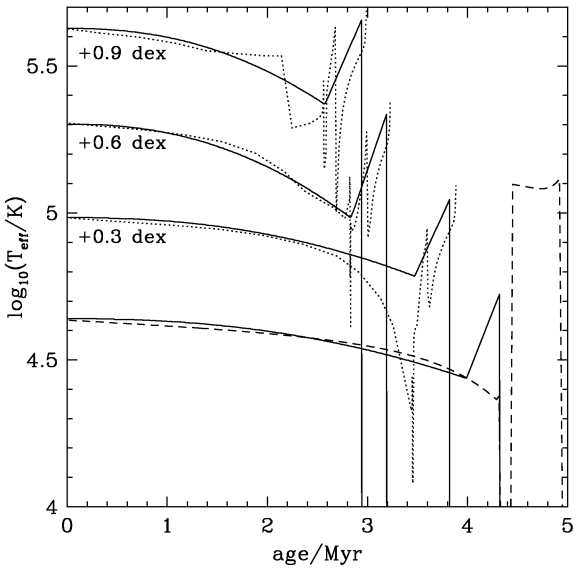

Figure B2. Effective temperature evolution for massive stars. The line styles are as in Fig. B1. As the $T_{\rm eff}$ for massive stars are rather similar, the lines in the plot have been shifted upwards as indicated in the plot.

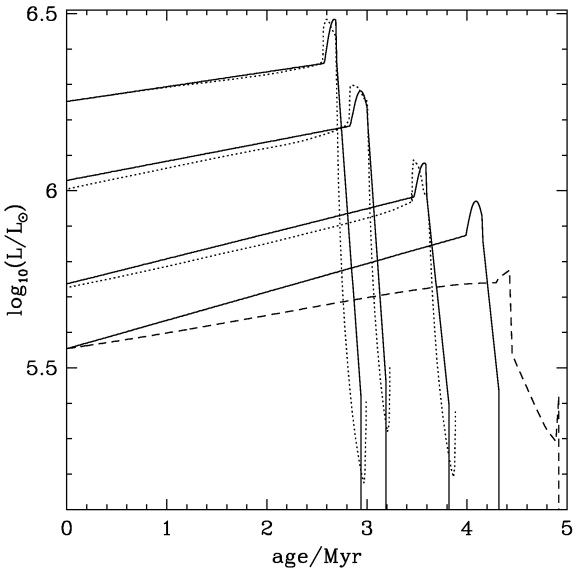

Figure B3. Luminosity evolution for massive stars. The line styles are as in Fig. B1.

For $\tau_{\rm m} < t < \tau_{\rm b}$

$$L(t) = L_{\rm jump} + (L_{\rm peak} - L_{\rm jump})\,\sin(L_{\rm sin}\,(t - \tau_{\rm m})). \quad \text{(B6)}$$

And finally for $\tau_{\rm b} \leqslant t \leqslant (\tau_{\rm m} + {\rm d}t)$

$$L(t) = a_4\,t + b_3. \quad \text{(B7)}$$

Here the parameters are

$$L_{\rm ini} = \frac{m_{\rm ini}}{M_L},$$

$$M_L = ml_{\rm m}\,m_{\rm ini} + ml_{\rm b},$$

$$L_{\rm jump} = \exp\left[\frac{L_{\rm je}}{(L_{\rm ini}^{L_{\rm pf}})}\right] + L_{\rm jc},$$

$$\tau_{\rm b} = \frac{1\times10^{-6}}{\tau_{\rm bb} - (\tau_{\rm bm}/m_{\rm ini})},$$

$$L_{\rm peak} = L_{\rm pa}\,\log_{10}\left(\frac{m_{\rm ini}}{L_{\rm pf}}\right) + L_{\rm pc},$$

$$a_4 = \frac{L_{\rm jump} - L_{\rm low}}{\tau_{\rm m} + {\rm d}t - \tau_b},$$

$$b_3 = L_{\rm low} - [a_4\,(\tau_{\rm m} + {\rm d}t)].$$

The constants are

$$ml_{\rm m} = 0.145\,590\,532,$$

$$ml_{\rm b} = 1.722\,994\,092,$$

$$L_{\rm je} = 9.0\times10^{-3},$$

$$L_{\rm pf} = 2.5,$$

$$L_{\rm jc} = 3.95,$$

$$\tau_{\rm bb} = 4.629\,6293\times10^{-7},$$

$$\tau_{\rm bm} = 1.1111\times10^{-5},$$

$$L_{\rm sin} = 15.7,$$

$$L_{\rm pa} = 1.35,$$

$$L_{\rm pc} = 4.215,$$

$$L_{\rm low} = 5.2.$$

Fig. B3 shows the results of the luminosity-fitting formulae.

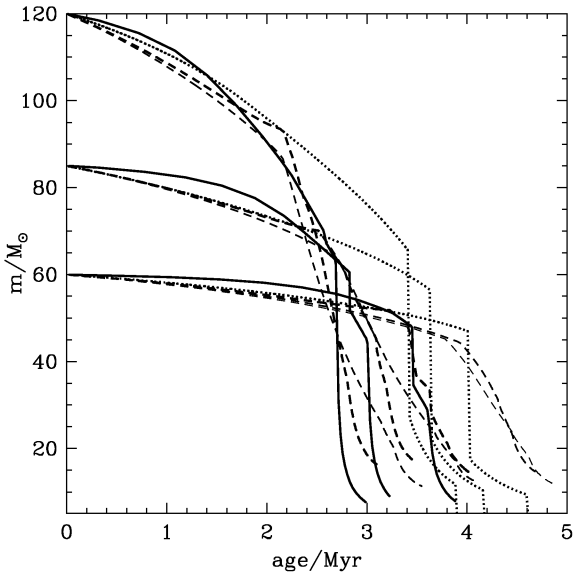

Figure C1. Stellar mass evolution for massive stars. The solid lines are the Geneva models (Schaller et al. 1992), while the dashed lines are the Geneva models with rotation (Meynet & Maeder 2003, thick-dashed line: no rotation, medium-dashed line: 300 km s^{-1}, thin-dashed line: 500 km s^{-1}, only for $m = 60\,{\rm M}_\odot$) and the results from the SSE package (Hurley et al. 2000) are shown as dotted lines.

APPENDIX C: COMPARISON OF DIFFERENT MODELS

Several different sets of theoretical models for stellar evolution of massive stars exist. Figs C1, C2 and C3 compare the mass, $T_{\rm eff}$ and luminosity evolution of three different sets of models (Schaller et al. 1992; Meynet & Maeder 2003; Hurley et al. 2000). These models agree qualitatively on the compared stellar properties but show minor differences in the details.

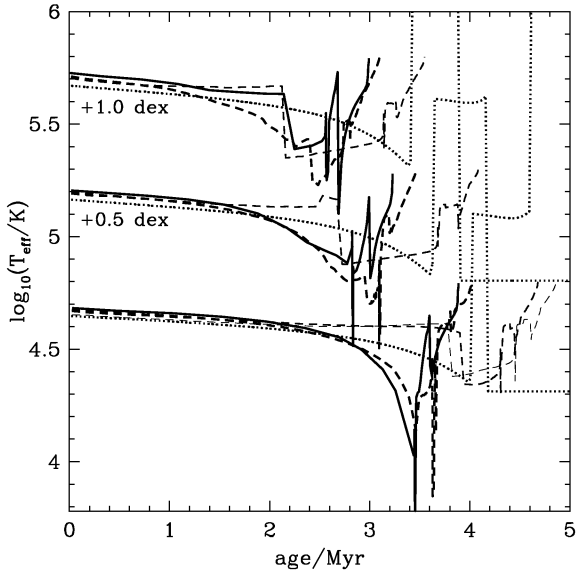

Figure C2. Effective temperature evolution for massive stars. The line styles are as in Fig. C1. As the $T_{\rm eff}$ for massive stars are rather similar, the lines in the plot have been shifted (as indicated in the plot) in the following way: the uppermost by +1.0 dex and the second one by +0.5 dex. The lowest plot has not been shifted.

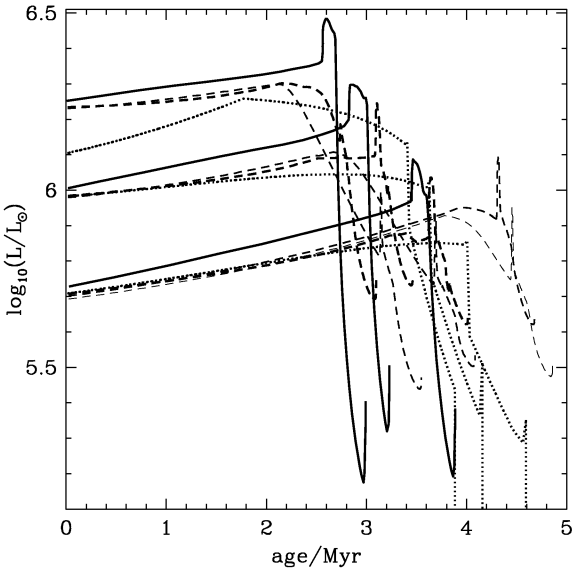

Figure C3. Luminosity evolution for massive stars. The line styles are as in Fig. C1.

This paper has been typeset from a TEX/LATEX file prepared by the author.